Archive of Applied Mechanics (2023) 93:2175–2189
https://doi.org/10.1007/s00419-023-02378-4

ORIGINAL

Marjan Noroozi · Aref Afsharfard · Masoud Tahani

Harvesting energy using simultaneous rotational and translational motions of a breakwater

Received: 8 July 2022 / Accepted: 7 February 2023 / Published online: 1 March 2023

Abstract Ocean wave energy is a dense, huge, and time-independent renewable energy resource. In the past decades, many types of research have been carried out to protect offshore and nearshore structures against ocean waves and convert this energy into useful energy. This study presents a reliable system that can break the waves and convert their energy into electricity. To do so, a mechanism with two plates, which can rotate and linearly move, is introduced. The plate motions are transmitted to the gearbox, whose output rotates a DC generator. In order to study the mechanical behavior of the presented mechanism, the governing equation of motion is derived and solved numerically. Numerical results are validated by experimental ones. Besides, the effect of changing the ocean wave properties on the output electrical power of the system is studied. Moreover, the wave transmission coefficients for the mechanism according to the different dimensionless incident wave numbers are experimentally obtained.

Keywords Ocean wave energy · Energy harvesting · Breakwater · Renewable energy · Wave energy converters

1 Introduction

Nowadays, tackling climate change, increasing global energy requests, and limited resources of fossil fuels cause renewable energies like solar, wave, and wind energy to attract attention [1–4]. Due to the density of renewable sources of energy, the first place is devoted to ocean wave energy [5]. It should be noted that wave energy can be exploited effectively up to 90% of the time, and oceans comprise around 71% of the earth's surface [6, 7]. Furthermore, the variation of the wave energy is aligned with the seasonal electricity demand and is more predictable than other resources like wind energy [8]. Besides, global wave power resource has been estimated to be at least 1 TW, with a potential annual energy production of about 2000 TWh [9]. Many wave energy converter (WEC) concepts are developed, but some are just discussed, others have become small-scale models, and few have been tested in the ocean [9].

It should be considered that deep water contains higher amounts of energy in comparison with shallow water. Therefore, WEC can harvest more amounts of energy in deep water. However, maintenance, construction, and survivability in extreme conditions are more difficult in the case of deep water than in shallow water [5, 10, 11]. According to the location of WECs, they are categorized into shoreline, nearshore, and offshore devices. In the LIMPET-based systems, classified as a shoreline WEC, which have an inclined chamber that is open from the bottom, the ocean waves travel toward the chamber and cause oscillation of the water column [5, 12–14].

M. Noroozi · A. Afsharfard (✉) · M. Tahani (✉)
Department of Mechanical Engineering, Faculty of Engineering, Ferdowsi University of Mashhad, Mashhad, Iran
e-mail: afsharfard@um.ac.ir

M. Tahani
e-mail: mtahani@um.ac.ir

This oscillation compresses and decompresses air and drives a wells turbine on top of the chamber [5, 12–14]. The oscillating wave surge converter (OWSC) is a nearshore WEC hinged to the sea bed. Waves interact with the plate and cause rotation along the hinge joint axis. These rotations pump water onshore to drive a hydraulic motor in a hydraulic system [15–17]. An example of offshore WECs is Pelamis, which consists of multiple cylindrical parts connected by hinge joints [18]. The rotational motion of the joint causes the pumping fluid into high-pressure accumulators and driving a variable displacement hydraulic motor [18, 19]. Overall, based on the energy harvesting method, the WECs can be classified into three groups [20]:

- Oscillating water columns (OWCs): are divided into fixed structures like Pico [21], LIMPET [22], Sakata [23], REWEC3 [24], Mutriku [25], and floating structures like Mighty Whale [26].
- Oscillating bodies: are classified into floating types like IPS buoy [27], Wavebob [28], AquaBuoy [29], Pelamis [18], SEAREV [30], and submerged types like AWS [31], Wave Roller [20], Oyster [32], and Mace [33].
- Overtopping devices: are categorized into fixed structures like TAPCHAN [34], SSG [35, 36], and floating structures like Wave Dragon [37].

Another classification for the WECs is according to their rigid or flexible bodies. The deformation of the flexible WECs with waves triggers an increase in efficiency and a decrease in structural damage risk compared to the rigid ones [38, 39].

On the other hand, hybridization is a solution to compensate for the excessive production costs of marine renewable energy and its intermittent nature. One way of hybridization is integrating multifunctional platforms and structures like breakwaters, oil and gas platforms, and aquaculture platforms with marine renewable energy technologies [40]. Practical devices can be introduced by combining the concepts of wave energy converters and breakwaters [41, 42]. Produced electrical energy can be consumed locally or transmitted. Zanuttigh et al. [43] considered OWC and Sea Slot-cone Generator (SSG), nearshore WECs, as breakwaters and analyzed their wave reflection based on experimental results. Thaha et al. [44] examined the magnitude of wave energy that can be harvested by creating a reservoir at the top crest of the rubble mound breakwater. When waves run up on the slope walls of the breakwater, the reservoir captures the over-topping discharge. Therefore, a pressure head is caused by different water levels between the reservoir and seawater level, which can generate power. Nabavi et al. [45] studied a low-volume piezoelectric beam-column connected to a vertical face as a breakwater and energy harvester. When the coming waves interact with the vertical face, they break, and their energy is converted to electricity via a piezoelectric beam-column.

This study suggests an efficient mechanism to break waves and harvest energy. This mechanism consists of two plates hinged together from one side. The first plate is hinged to the fixed frame from another side and only can rotate about this side. The second plate's other side can translate on a straight path on the frame and rotate about this side. The translational side of the plate is connected to a spring that is connected to the fixed frame. When waves interact with these plates, there are several rotational and one translational motion. The translational motion of this mechanism is used to generate electricity via an array of gears and a DC generator. These gears convert the two-side translational motion to one-side rotational motion. For this aim, a horizontal plate is attached to the second plate's translating side on a straight path and only translates. Two racks are attached to this plate from one side. Since each rack is engaged with a pinion, the translational motions of the racks are converted to the rotational motions of the pinions in opposite directions. Also, two gears mounted on a shaft are engaged with these two pinions. As translational motion is reciprocating and the direction of rotation of the gears alters, between the shaft and each gear, a one-way bearing is placed to transmit the rotation in one direction. Accordingly, the coupled shaft with the DC generator rotates in one direction and generates electricity. This feasible, reliable, and affordable mechanism can stand against waves similar to the vertical wall breakwaters to a certain extent and converts the surge motion of the waves to the linear motion to produce electricity.

2 Mathematical modeling

As shown in Fig. 1, consider two plates of width a, length l, thickness t, mass m, and the moment of inertia about an axis that passes through the center of mass of the plate and is parallel to its axis of rotation $\overline{I}$. The stiffness of the spring is k. θ is the angle of rotation of the plates about their sides which are not hinged together, and $\dot{\theta}$ is the rotational velocity.

As shown in Fig. 2, F_w is the resultant force of the pressure applied to each plate's center of mass. Since this mechanism is one degree of freedom, the position of the plates can be determined by θ.

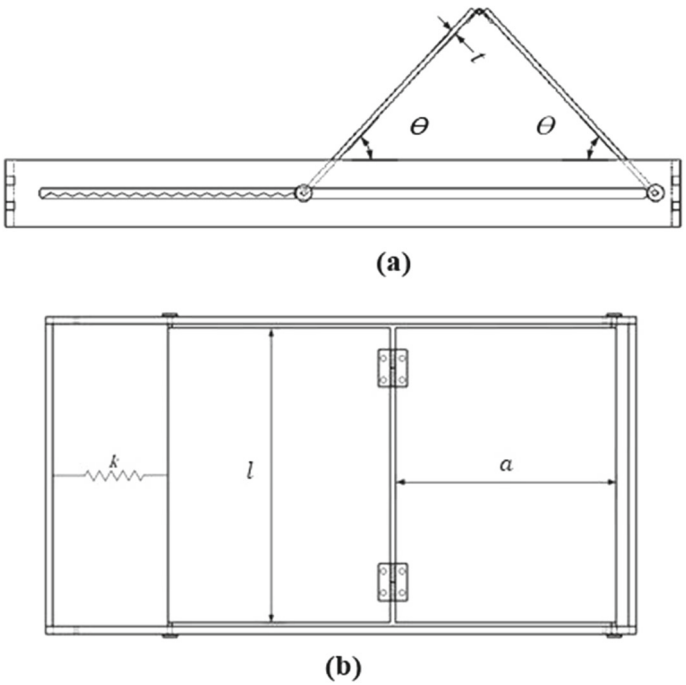

Fig. 1 A schematic of **a** the top view of the mechanism when there is an angle of rotation and **b** its front view when the rotation angle is zero

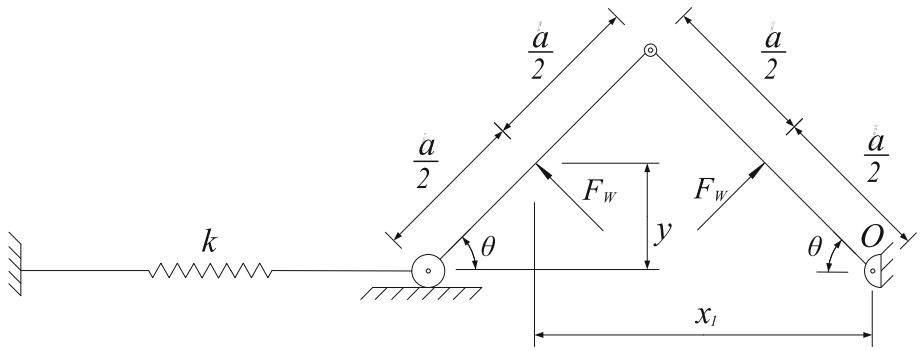

Fig. 2 A schematic of the mechanism from the top view

Note that x_1 and y are, respectively, horizontal and vertical coordinates of the translating plate's center of mass and can be given by:

$$x_1 = \frac{3a}{2}\cos\theta \tag{1-1}$$

$$y = \frac{a}{2}\sin\theta \tag{1-2}$$

Furthermore, $\dot{x}_1$ and $\dot{y}$ are, respectively, the Cartesian components of the velocity of the translating plate's center of mass and are equal to:

$$\dot{x_1} = -\frac{3a}{2}\dot{\theta}\sin\theta \tag{2-1}$$

$$\dot{y} = \frac{a}{2}\dot{\theta}\cos\theta \tag{2-2}$$

The elongation of the spring and the velocity of the spring's endpoint are as follows:

$$x_2 = 2a(1-\cos\theta) \tag{3-1}$$

Table 1 Values of the apparent increase in mass for rectangular cylinders in translation parallel to a side against different ratios of the width of the plate to the mean length of the plate is covered by water [47]

a/d	0	0.025	0.111	0.298	0.676	1.478	3.555	9.007	40.03
$M_1''/(\rho\pi d^2/4)$	1	1.05	1.16	1.29	1.42	1.65	2.00	2.50	3.50

$$\dot{x}_2 = 2a\dot{\theta}\sin\theta \tag{3-2}$$

Also, the potential energy equation is as follows:

$$U = \frac{1}{2}k(x_2 + p_t)^2 \tag{4}$$

where p_t is the change in the initial length of the spring at $\theta = 0$. The total work done by external loads is as follows

$$W = -F_w x_2 \sin\theta + F_w a\theta \tag{5}$$

The kinetic energy of the mechanism is

$$T_1 = \frac{1}{2}I_o\dot{\theta}^2 + \frac{1}{2}\bar{I}\dot{\theta}^2 + \frac{1}{2}m\left(\dot{x}_1^2 + \dot{y}^2\right) + \frac{1}{2}\frac{m_s}{3}\dot{x}_2^2 \tag{6}$$

A submerged vibrating structure in fluid leads to surrounding fluid displacement. Accordingly, fluid pressures are generated, and a hydrodynamic force acts on the structure. The vibrations of the structure in the fluid change dynamics of the vibrating structure, particularly its natural frequency and damping characteristics. It should be noted that the hydrodynamic mass changes natural frequency, and the damping effect is related to viscous loss and acoustic radiation [46]. Added masses and corresponding kinetic energies are calculated for these mechanism motions. The kinetic energy of the added mass [47] for two-dimensional potential flow (added mass kinetic energy per unit length normal to the plane) is due to the rotation of a plate about its one side (T_{11}), rotation of a plate about its center of mass (T_{12}), displacement in the vertical direction (T_{13}), and displacement in the horizontal direction (T_{14}), which are equal to:

$$T_{11} = \frac{9}{16}\rho\pi\left(\frac{a}{2}\right)^4\dot{\theta}^2 \tag{7}$$

$$T_{12} = \frac{1}{16}\rho\pi\left(\frac{a}{2}\right)^4\dot{\theta}^2 \tag{8}$$

$$T_{13} = \frac{1}{2}\rho\pi\left(\frac{a}{2}\right)^2\dot{y}^2 \tag{9}$$

$$T_{14} = \frac{1}{2}M_1''\dot{x}_1^2 \tag{10-1}$$

where ρ is the water density, and M_1'' is an apparent increase in mass which can be determined by the width of the plate and the mean length of the plate covered by water d. (Due to the fluctuations which occur on the water surface in the presence of the waves, the mean length is considered.) M_1'' for different ratios of $\frac{a}{d}$ is presented in Table 1.

In this case, $\frac{a}{d}$ equals 1.4114, and this ratio is between 0.676 and 1.478. So, by applying linear interpolation M_1'' is

$$M_1'' = 1.6309\frac{\rho\pi d^2}{4} \tag{10-2}$$

Substituting Eq. (10-1) into Eq. (10-2) results in:

$$T_{14} = 0.8154\left(\frac{\rho\pi d^2}{4}\right)\dot{x}_1^2 \tag{10-3}$$

Therefore, total kinetic energy is equal to:

$$T = T_1 + T_{11}d + T_{12}d + T_{13}a + T_{14}t \tag{11}$$

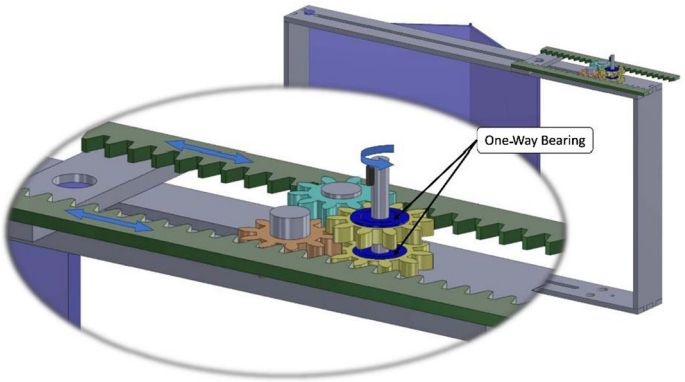

Fig. 3 A schematic view of an array of gears and one-way bearings integrated with the mechanism

Lagrange's equation can be expressed as:

$$\frac{d}{dt}\left(\frac{\partial T}{\partial \dot{\theta}}\right) - \frac{\partial T}{\partial \theta} + \frac{\partial U}{\partial \theta} = Q \tag{12}$$

where Q is the generalized force. Substituting Eqs. (4), (5), and (11) into Eq. (12), the equation of motion of the mechanism is obtained as

$$\begin{aligned}
&\Big(I_0 + \bar{I} + 2ma^2\sin^2\theta + \frac{ma^2}{4} + \frac{4}{3}m_s a^2\sin^2\theta + \frac{5}{64}\rho\pi a^4 d + \frac{1}{16}\rho\pi a^5\cos^2\theta \\
&\quad + 0.9173\rho\pi a^2 d^2 t\sin^2\theta\Big)\ddot{\theta} \\
&+\Big(ma^2\sin 2\theta + \frac{2}{3}m_s a^2\sin 2\theta - \frac{1}{32}\rho\pi a^5\sin 2\theta + 0.4586\rho\pi a^2 d^2 t\sin 2\theta\Big)\dot{\theta}^2 \\
&+4ka^2\sin\theta - 2ka^2\sin 2\theta + 2aF_w\sin^2\theta - F_w a + 2kap_t\sin\theta = 0
\end{aligned} \tag{13}$$

In the next step, an array of gears and two one-way bearings are integrated with this mechanism, as shown in Fig. 3. In consequence of connecting the shaft to a DC generator, a novel system can be introduced which generates electricity.

In order to present the equations, the system is divided into two separate parts from the location where the horizontal plate is attached to the racks. Therefore, F_t can be defined as a force between the horizontal plate and racks. To this end, Eq. (13) will alter to:

$$\begin{aligned}
&\Big(I_0 + \bar{I} + 2ma^2\sin^2\theta + \frac{ma^2}{4} + \frac{4}{3}m_s a^2\sin^2\theta + \frac{5}{64}\rho\pi a^4 d + \frac{1}{16}\rho\pi a^5\cos^2\theta \\
&\quad + 0.9173\rho\pi a^2 d^2 t\sin^2\theta + 4m_{plate}a^2\sin^2\theta\Big)\ddot{\theta} \\
&+\Big(ma^2\sin 2\theta + \frac{2}{3}m_s a^2\sin 2\theta - \frac{1}{32}\rho\pi a^5\sin 2\theta + 0.4586\rho\pi a^2 d^2 t\sin 2\theta + 2m_{plate}a^2\sin 2\theta\Big)\dot{\theta}^2 \\
&+4ka^2\sin\theta - 2ka^2\sin 2\theta + 2aF_w\sin^2\theta - F_w a + 2kap_t\sin\theta + 2aF_r\sin\theta = 0
\end{aligned} \tag{14}$$

where m_{plate} is the mass of the horizontal plate. Moreover, the array of gears and the DC generator are considered as a set to present the equations. As pinions and gears are alike in that each has ten teeth, the angular velocities of the engaged gears are equal and are expressed with Ω. The pitch radius of the pinion is r_p. The velocity of the spring's endpoint equals the velocity of a rack engaged with a pinion according to the following equation:

$$\dot{x}_2 = r_p\Omega \tag{15}$$

The rotation of the coupled shaft with the DC generator is aligned with the rotation of the gears. Accordingly, the pinions, gears, shaft, and DC generator have the same angular velocities. J_p and J_s are the moment of

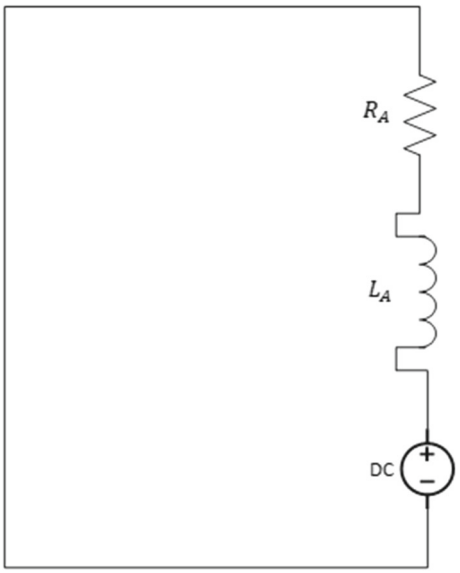

Fig. 4 The electrical circuit of the generator

inertia of each pinion and the moment of inertia of each gear, respectively. The mass of each rack is m_{rack}. The moment of inertia of the motor is expressed with J_m. So, the total kinetic energy of the gears combined with the DC generator can be written as

$$T_s = \left(J_p + m_{\text{rack}} r_p^2\right)\Omega^2 + J_s\Omega^2 + \frac{1}{2}J_m\Omega^2 \tag{16}$$

Since the total kinetic energy of the set is

$$T_s = \frac{1}{2}J_T\Omega^2 \tag{17}$$

the total moment of inertia of the set is obtained as

$$J_T = 2\left(J_p + m_{\text{rack}} r_p^2\right) + 2J_s + J_m \tag{18}$$

Regarding Newton's law, the mechanical equation of the motor is

$$J_T\dot{\Omega} + C_1\Omega = T_{in} - T_{\text{emf}} \tag{19}$$

where C_1 is the intrinsic rotational damping of the DC generator and T_{in} is the input torque that can be expressed as

$$T_{in} = r_p F_t \tag{20}$$

Also, k_b and I are the back electromotive force constant of the generator and generated current by the generator, respectively. Therefore, the torque of the back electromotive force can be presented as

$$T_{\text{emf}} = k_b I \tag{21}$$

The electrical circuit of the generator is shown in Fig. 4. L_A is the inductance of the DC generator, and R_A is its resistance. Based on Kirchhoff's voltage law, the following equation can be written:

$$k_b\Omega - L_A\dot{I} - R_A I = 0 \tag{22}$$

In this study, wave force is obtained by using Airy wave theory and Bernoulli's equation. Airy wave theory comprises the solution of the linear equation of the continuity for an irrotational flow and the utilization of linearized boundary conditions. Wave parameters are shown in Fig. 5. The origin of the Cartesian coordinate system is considered on the still water level (SWL), which is the calm-water position. The measured distance

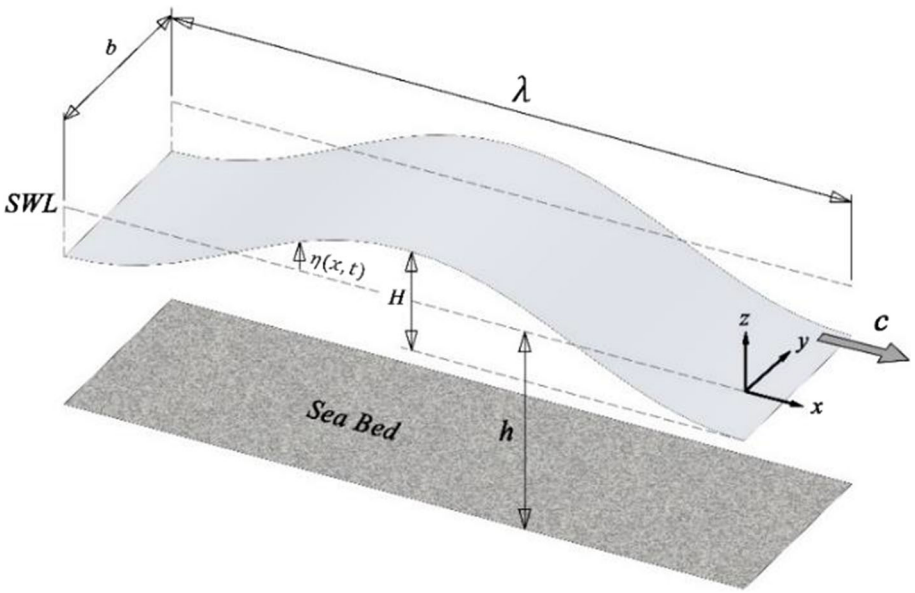

Fig. 5 Sketch and notation for the linear wave parameters

from the seabed to the SWL is water depth, h. The distance from trough to crest of the wave is called wave height, H. The wavelength, λ, is from crest to crest, as shown. The wavenumber, K, equals $\frac{2\pi}{\lambda}$. The celerity or phase velocity at which the wave travels in the x-direction is c. Vertical free surface displacement,$\eta(x, t)$, is measured from SWL as indicated [48]. Airy wave theory can be applied when the wave steepness ($\frac{H}{\lambda}$) is much less than the unit.

Based on the Airy wave theory, the following parameters are expressed. Velocity potential for traveling or progressive waves can be written in terms of the circular wave frequency,ω, as follows [48]:

$$\phi = \frac{H}{2}\frac{g}{\omega}\frac{\cosh[K(z+h)]}{\cosh(Kh)}\sin(Kx - \omega t) \tag{23}$$

where g is the gravitational acceleration. The circular wave frequency is [48]

$$\omega = \sqrt{gK\tanh Kh} \tag{24}$$

Vertical displacement of a wave particle about a fixed line with the distance z from SWL on the Cartesian coordinate system can be written as [48]

$$\eta(x, z, t) = \frac{H}{2}\frac{\sinh[K(z+h)]}{\sinh(Kh)}\cos(Kx - \omega t) \tag{25}$$

Moreover, based on the Airy wave theory and Bernoulli's equation, the pressure which a wave particle applies during its progress is as follows [48]:

$$p = -\rho\frac{d\phi}{\mathrm{d}t} - \rho g(z + \eta(x, z, t)) \tag{26}$$

Integrating Eq. (26) over the surface of a plate covered by water leads to the wave force acting upon this plate as:

$$F_w = \int pdA = \int_{-d}^{0} padz = \frac{\rho g H a}{2K}\left[\tanh(Kh) - \coth(Kh) - \frac{\sinh[K(h-d)]}{\cosh(Kh)} + \frac{\cosh[K(h-d)]}{\sinh(Kh)}\right] \cos(Kx - \omega t) + \frac{\rho g a d^2}{2} \tag{27}$$

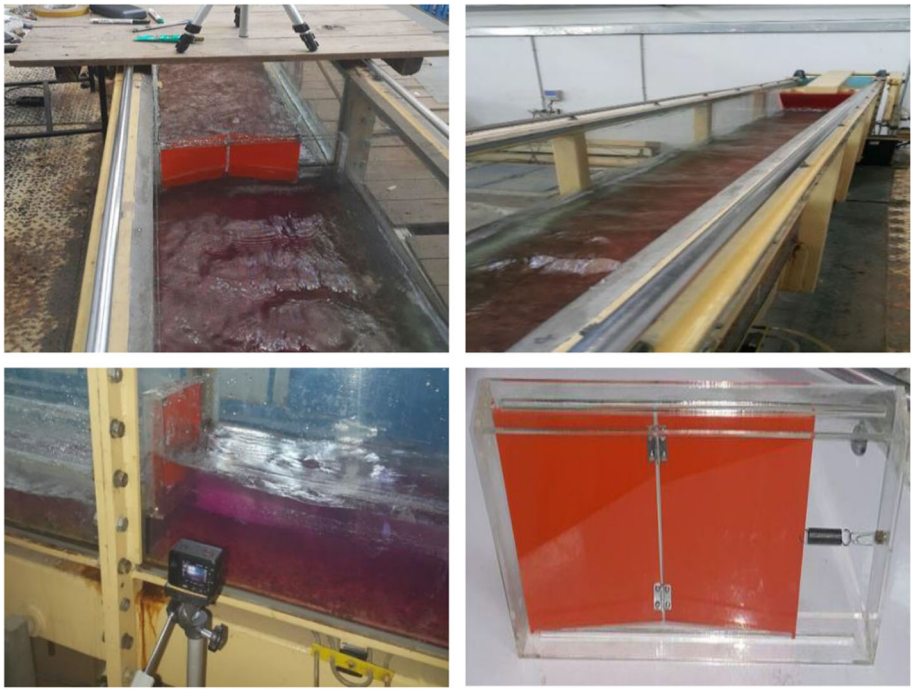

Fig. 6 Setup of the experimental model in the wave flume

Table 2 Intermediate water wave parameters

Wave parameter	H(m)	λ(m)	K(rad/m)	h(m)	ρ(kg/m^3)
Magnitude	0.0393	0.8332	7.5406	0.1817	1000

Table 3 Prototype structural parameters

Prototype structural parameter	I_0(gr.m^2)	$\overline{I}$(gr.m^2)	m(kg)	a(m)	l(m)	t(m)	k(N/m)
Magnitude	0.8175	0.2072	0.1085	0.15	0.2	0.003	300

An insightful expression of the above equation is made through Fig. 08 presenting dimensionless wave force amplitude number $\frac{A_{F_w}}{\rho g H a d}$ according to the dimensionless wave number Kh. A_{F_w} is the wave force amplitude for each particular wave.

Wave transmission occurs when the wave energy passes over, under, or through a breakwater. Therefore, the transmitted wave behind the breakwater contains less energy than the incident wave that interacts with the breakwater. The wave transmission coefficient, which shows the amount of wave transmission, is defined as the ratio of the transmitted wave height, H_t, to the incident wave height, H_i [49, 50]:

$$C_t = \frac{H_t}{H_i} \tag{28}$$

3 Experimental study

In the absence of an array of gears and the DC generator, a physical model of the mechanism was simulated in the Hydraulic Laboratory of the Ferdowsi University of Mashhad. The proposed mechanism was made from plexiglass and was placed in the $800 \times 50 \times 40$cm wave flume, as shown in Fig. 6. The mechanism was located at the middle of the flume and was elevated 7.5 cm from the flume bed. The simulation was conducted in the cases of intermediate water. Wave and prototype structural parameters are given in Tables 2 and 3.

Table 4 Infinite range of $\frac{h}{\lambda}$ classification

Shallow water	Intermediate water	Deepwater
$\frac{h}{\lambda} \leq \frac{1}{20}$	$\frac{1}{20} < \frac{h}{\lambda} < \frac{1}{2}$	$\frac{h}{\lambda} \geq \frac{1}{2}$

Table 5 The structural parameters of the DC generator

Parameter	$R_A(\Omega)$	L_A(mH)	k_b(V.s/rad)	J_m(kg.mm^2)	C_1(N.m.s/rad)
Magnitude	9	24	0.0458	0	0

Table 6 The structural parameters of the gears

Parameter	J_p(kg.mm^2)	J_s(kg.mm^2)	r_p(m)	m_{rack}(kg)
Magnitude	71.0358	26.4047	0.01	0.0031

Table 7 Intermediate water wave parameters

Wave parameter	H(m)	λ(m)	K(rad/m)	h(m)	ρ(kg/m^3)
Magnitude	0.0508	0.5073	12.3848	0.1845	1000

The mean length of the plate covered by water depth d and spring pretension force F_{p_t} are, respectively, equal to 0.1067 m and 2.4 N. In ocean engineering, an infinite range of $\frac{h}{\lambda}$ is classified into three regions, as given in Table 4. Based on this classification, this study was conducted in the intermediate water condition where the surge motion of the waves is exaggerated [48, 51, 52]. This place is desirable for this WEC exploiting the surge motion of the waves (Tables 5 and 6).

4 Results and discussion

In order to perform a numerical simulation of the system, in the first stage, the mechanism is modeled using CAD software based on the dimensions presented in Table 3. In the next stage, it is imported into the multibody dynamics simulation software and integrated with a gear train. The spring connecting the second plate to the frame is added, and the required constraints are applied. Besides, the wave force acting on each plate's center of mass is defined. By defining each element's density, this software calculates the required structural characteristics of the elements. In the third stage, the modeled system in multibody dynamics simulation software is imported to the toolbox Simulink of MATLAB software as a block diagram representing the wave force as input and angular velocities of the gears and the rotation angle of the plates as outputs. The angular velocities of the gears are used as inputs to convert the two-way rotations of the gears to a one-way rotation. Afterward, this one-way rotation is used as input for the electrical circuit of the generator modeled using Simscape elements of the MATLAB software. A wave with characteristics given in Table 7 is simulated in the laboratory. It is assumed that the mean length of the plate covered by water is about 0.05 m in this case. Accordingly, when the wave troughs reach the plates, there is no force on the plates, and the rotation angle of the plates is zero. The parameters of the DC generator and gears required for modeling this system are given in Tables 5 and 6. The structural parameters of the DC generator are obtained via the experiment. In addition, it is assumed that the gears are made of PLA, whose density is 1250 kg/m^3. Ultimately, results from this three-stage simulation can be compared to those obtained from the numerical solution of the coupled electromechanical equations. It should be noted that in this simulation, the added masses of the water and the mass of the spring are neglected.

As shown in Fig. 7, the wave force acting on each plate of the mechanism varies between 8.052 and 8.708 N. These results are obtained via numerical solution of the mechanical equations of the mechanism using the Simulink toolbox of the MATLAB software (auto solver and time fixed step size 0.001 s) and experimental study by considering the wave parameters given in Table 2. Moreover, Fig. 8 endeavors to convey a better understanding of Eq. (27) via non-dimensional analysis. It should be noted that every wave has its particular

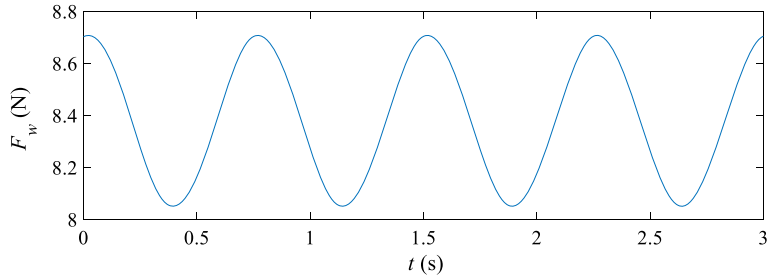

Fig. 7 The wave force acting on the plates of the mechanism according to the time based on parameters given in Table 2

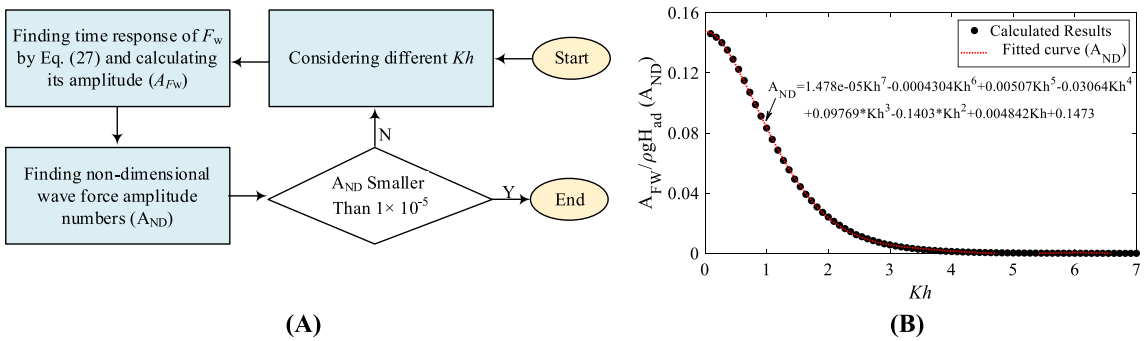

Fig. 8 Procedure of finding dimensionless wave force amplitude (A_{ND}) acting on each plate (**A**); and variation of A_{ND} versus the dimensionless wave number (**B**)

characteristics, as shown in Fig. 7 as an example. By the variation of Kh, these characteristics alter, and they become new waves. Wave force and wave force amplitudes ($A_{F_w} = \frac{(F_w)_{max}-(F_w)_{min}}{2}$) by the variation of Kh are obtained, and the wave force amplitudes are non-dimensionalized. In part (A) of Fig. 8, procedure of finding the non-dimensional wave force amplitude numbers ($A_{ND} = \frac{A_{Fw}}{\rho g H a d}$) is presented. Variation of the A_{ND} versus the non-dimensional wave numbers (Kh) is demonstrated in part (B) of Fig. 8. Moreover, when Kh tends to 0 means that K tends to 0 (for having still water level h cannot tend to 0). Thus, regarding Eq. (24), λ and ω will tend toward infinity and 0, respectively. Therefore, there will be still water with a wave force amplitude of 0 [48]. The maximum dimensionless wave force amplitude is 0.146 for 0.0901 dimensionless wave number.

This mechanism is one degree of freedom. Accordingly, the translating plate's translational motion about its one side connected to the spring (x_2) is related to the rotation angle (θ). As shown in Fig. 9(a), this motion is obtained experimentally via a camera and tracker video analysis software which allows the analysis of the particle (or body) motion frame by frame and theoretically regarding Eq. (13). Experimental results confirm numerical ones. The difference between theoretical and experimental results in this physical modeling stems from the damping, friction, viscous, and eddy losses. In addition, the error between the experimental and calculated added masses can trigger the difference between the frequencies. Human, instruments, and the environment are the three other major sources of error. As shown in Fig. 9, there are small and large peaks per period. The theoretical angle of rotation varies between about 0.3211 and 0.4152 rad. The translational motion of the translating plate's side attached to the spring is between about -0.0013 and 0.0088 m in the case of the theoretical result, and its period equals the angle of rotation's period. The negative values for x_2 means that the rotation angle is less than the initial angle of rotation. Also, experimental results for this motion vary between about -0.0002 and 0.0070 m.

As shown in Fig. 10, five experimental data are obtained to analyze energy transmission from this breakwater. Dimensionless wave transmission coefficient varies between 0.5151 and 0.7782, while dimensionless incident wave number varies between 1.0100 and 2.3232. The minimum wave transmission coefficient, which means transferring the minimum wave energy from this breakwater, equals 0.5151 for a 1.7993 dimensionless incident wave number.

Table 8 indicates measured transmitted and incident wave heights, Wave transmission coefficient, and dimensionless incident wave number for the process of breaking a wave.

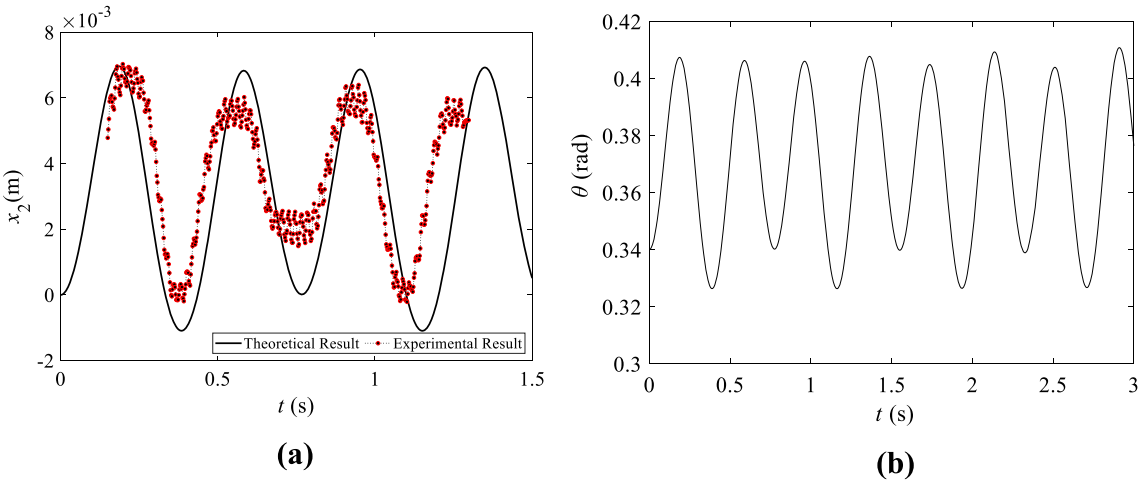

Fig. 9 Time histories of **a** translational motion of translating plate's side connected to the spring and **b** theoretical angle of rotation of the plates

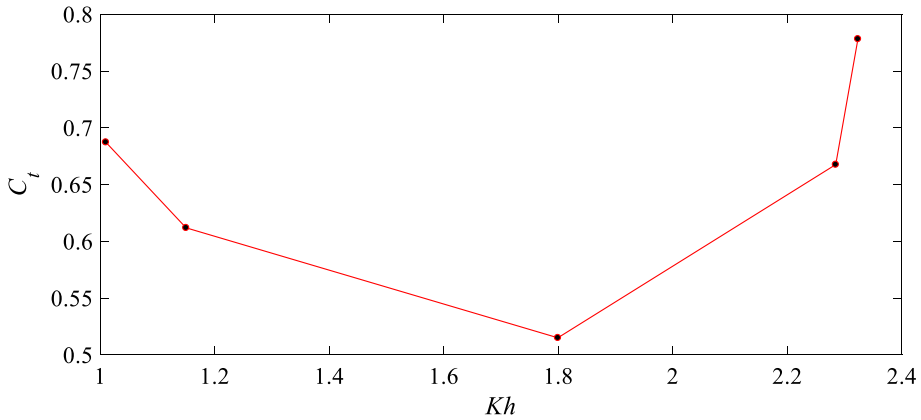

Fig. 10 Wave transmission coefficient (C_t) according to the dimensionless incident wave number (Kh)

Table 8 Incident and transmitted wave parameters

Wavenumber	1	2	3	4	5
Dimensionless incident wave number (Kh)	1.0100	1.1501	1.7993	2.2844	2.3232
Incident wave height (H_i)	0.0646	0.0581	0.0660	0.0508	0.0310
Transmitted wave height (H_t)	0.0444	0.0356	0.0246	0.0339	0.0241
Wave transmission coefficient (C_t)	0.6873	0.6120	0.5151	0.6677	0.7782

The wave force acting on each plate of the integrated system is calculated based on parameters given in Table 7 and is shown in Fig. 11. The coupled electromechanical equations of the system are solved numerically via Simulink toolbox (auto solver and time fixed step size 0.001 s) and compared to those obtained via co-simulation, as shown in Figs. 12 and 13.

Theoretical and simulation results are close together in conformity with the expectations. The difference is due to the applying different numerical methods in solving equations and the simulation. The theoretical displacement of the attached side of the second plate to the spring varies between 0 and 0.014 m, while the simulated displacement alters from 0 to 0.016 m. The rotation angle changes from 0 to 0.31 rad, theoretically. In contrast, it varies from 0 to 0.33 rad based on simulation results. The theoretical and simulation results for the angular velocity of the generator alter from 0 to 36 and 39 rad/s, respectively. In addition, the theoretically generated power changes from 0 to 0.2973 W, while the result obtained from simulation varies from 0 to 0.3557 W. This power is adequate for this small-scale energy harvester and can be increased significantly

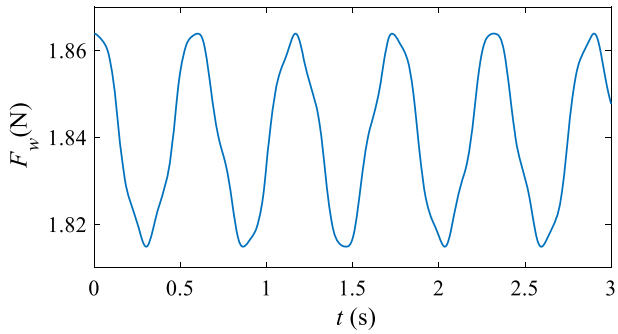

Fig. 11 The wave force acting on the plates of the mechanism according to the time based on parameters given in Table 7

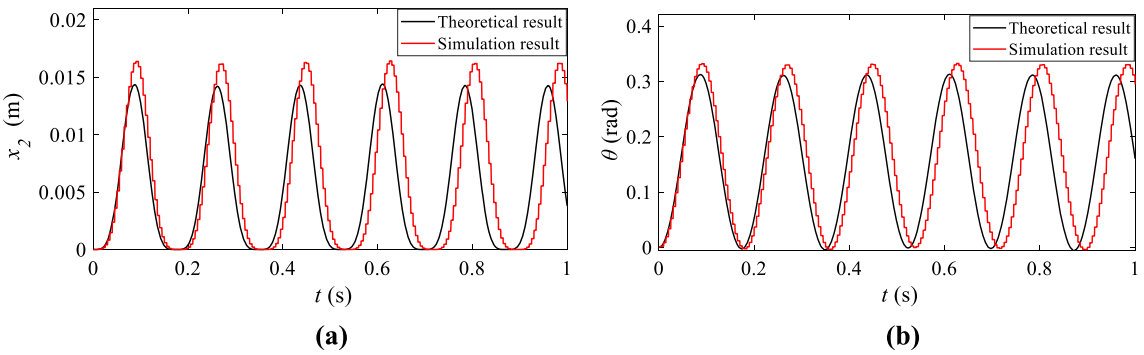

Fig. 12 Time histories of **a** displacement of the translating plate's side connected to the spring and **b** rotation angle of the plates

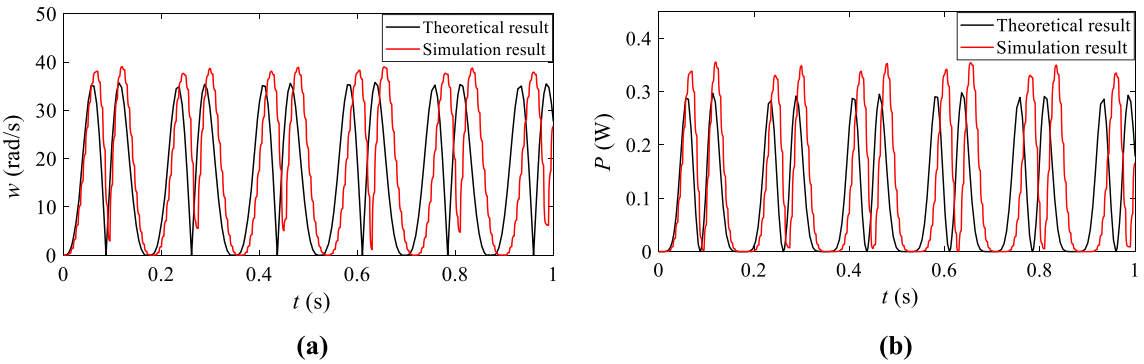

Fig. 13 Time histories of **a** angular velocity of the DC generator and **b** generated power by the DC generator

for the real-scale energy harvester. By considering common scaling factors for WECs, the scaling factors for converting the power and wave period of the small-scale model into the real-scale version are $s^{3.5}$ and $s^{0.5}$, respectively, where s is the geometrical scale factor [53]. According to Table 7 and Eq. (24), the frequency of the simulated wave is 1.091×10^{1} rad/s, and its period is 5.759×10^{-1} s. For this wave and a wave in the Persian Gulf whose period is 5.6 s [54], the geometrical scale of 9.455×10^{1} is obtained using the wave period scaling factor. So, by applying the power scaling factor, the generated power of the real-scale version will alter from 0 to about 2.923 MW.

The maximum theoretical power can be generated by harvesting wave energy using the presented system according to the dimensionless number $\frac{h}{gT^2}$ which is shown in Fig. 14. The water depth,h, is considered constant and equals 0.1844 m, while the wave period, T, is variable. When the dimensionless number is 0.5401, the maximum generated power reaches its highest amount of 0.3832 W. Therefore, the optimal amount of wave period is 0.1865s.

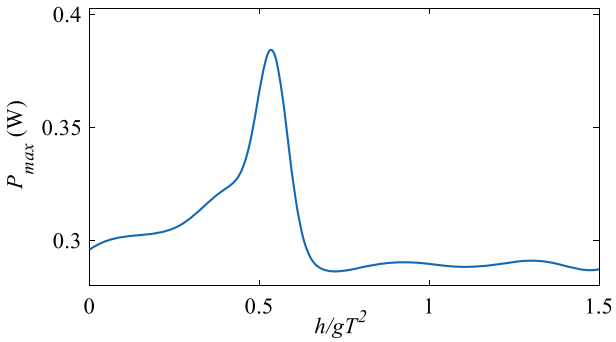

Fig. 14 Max theoretical generated power according to the dimensionless number $\frac{h}{gT^2}$

5 Conclusions

Not only does the novel introduced mechanism in this study work as a breakwater, but also it can harvest energy. The mechanical behavior of the mechanism is theoretically modeled and then validated by experiment. It is shown that the wave transmission coefficient of the mechanism, which is experimentally obtained according to the dimensionless incident wave number of 1.7993, is the minimum value. Also, it is experimentally observed that translating side of the plate moves about 7 mm, which is enough for a small energy harvesting system. Using a gearbox and a DC generator, the linear motion of the wave breakers is converted to electrical energy. It is shown that the presented small-scale system generates 2.973×10^{-1}W that could be increased to more than 3.8×10^{1}W when the dimensionless number of h/gT^2 is equal to 5.401×10^{-1}. Based on the non-dimensional analysis, the real-scale model in the Persian Gulf would generate about 2.923 MW. Finally, it can be concluded that the suggested system is a practical energy harvester that can efficiently break ocean waves.

References

1. Wang, L., Zhao, T., Lin, M., Li, H.: Towards realistic power performance and techno-economic performance of wave power farms: the impact of control strategies and wave climates. Ocean Eng. **248**, 110754 (2022)
2. Ahamed, R., McKee, K., Howard, I.: A review of the linear generator type of wave energy converters' power take-off systems. Sustainability **14**, 9936 (2022)
3. Gu, C., Li, H.: Review on deep learning research and applications in wind and wave energy. Energies **15**, 1510 (2022)
4. Arguilé-Pérez, B., Ribeiro, A.S., Costoya, X., deCastro, M., Carracedo, P., Dias, J.M., Rusu, L., Gómez-Gesteira, M.: Harnessing of different WECs to harvest wave energy along the galician coast (NW Spain). J. Marine Sci. Eng. **10**(6), 719 (2022)
5. Drew, B., Plummer, A.R., Sahinkaya, M.N.: "A Review of Wave Energy Converter Technology. Sage Publications Sage, UK (2009)
6. Xu, R., Wang, H., Xi, Z., Wang, W., Xu, M.: Recent progress on wave energy marine buoys. J Marine Sci Eng **10**, 566 (2022)
7. Kang, H.-G., Lee, Y.-H., Kim, C.-J., Kang, H.-D.: Design optimization of a cross-flow air turbine for an oscillating water column wave energy converter. Energies **15**, 2444 (2022)
8. Hernández, J., García, D., Varona, H.L., Calzada, A.E., Rodriguez, A., Reyes, D., et al.: Wave energy: state of the art and current development. Pan-Am. J. Aquatic Sci. **17**, 176–189 (2022)
9. Titah-Benbouzid, H., Benbouzid, M.: An up-to-date technologies review and evaluation of wave energy converters. Int. Rev. Electric. Eng.-IREE. **10**(1), 52–61 (2015)
10. Liu, W., Liu, L., Wu, H., Chen, Y., Zheng, X., Li, N., Zhang, Z.: Performance analysis and offshore applications of the diffuser augmented tidal turbines. Ships Offshore Struct. **18**(1), 68–77 (2023)
11. Lu, S., Ban, Y., Zhang, X., Yang, B., Yin, L., Liu, S., Zheng, W.: Adaptive control of time delay teleoperation system with uncertain dynamics. Front. Neurorobot. **22**, 152 (2022)
12. C. B. Boake, T. J. Whittaker, M. Folley, and H. Ellen, "Overview and initial operational experience of the LIMPET wave energy plant." In the twelfth international offshore and polar engineering conference, 2002.
13. Mishra, S., Purwar, S., Kishor, N.: Maximizing output power in oscillating water column wave power plants: an optimization based MPPT algorithm. Technologies **6**, 15 (2018)
14. Chen, Z., Liu, Z., Yin, L., Zheng, W.: Statistical analysis of regional air temperature characteristics before and after dam construction. Urban Climate **41**, 101085 (2022)
15. Schmitt, P., Windt, C., Nicholson, J., Elsässer, B.: Development and validation of a procedure for numerical vibration analysis of an oscillating wave surge converter. European J. Mech.-B/Fluids **58**, 9–19 (2016)
16. Amini, E., Asadi, R., Golbaz, D., Nasiri, M., Naeeni, S.T., Majidi Nezhad, M., Piras, G., Neshat, M.: Comparative study of oscillating surge wave energy converter performance: a case study for southern coasts of the Caspian Sea. Sustainability. **13**(19), 10932 (2021)

17. Liu, Z., Wang, Y., Hua, X.: Prediction and optimization of oscillating wave surge converter using machine learning techniques. Energy Convers. Manage. **210**, 112677 (2020)
18. Yemm, R., Pizer, D., Retzler, C., Henderson, R.: Pelamis: experience from concept to connection. Philosophic. Trans. Royal Soc. A: Mathemat. Phys. Eng. Sci. **370**, 365–380 (2012)
19. Al-Habaibeh, A., Su, D., McCague, J., Knight, A.: An innovative approach for energy generation from waves. Energy Convers. Manage. **51**, 1664–1668 (2010)
20. Antonio, F.D.: Wave energy utilization: a review of the technologies. Renew. Sustain. Energy Rev. **14**(3), 899–918 (2010)
21. Falcão, A.F., Sarmento, A.J., Gato, L.M., Brito-Melo, A.: The Pico OWC wave power plant: Its lifetime from conception to closure 1986–2018. Appl. Ocean Res. **98**, 102104 (2020)
22. D. Pradhan, "Shoreline wave energy converted to electrical energy with help of LIMPET technology and its assessment," J. Renew. Energy Resour 1: 2.
23. S. Takahashi, H. Nakada, H. Ohneda, and M. Shikamori, "Wave power conversion by a prototype wave power extracting caisson in Sakata port."Coastal Eng. 1992, 1993: 3440–3453.
24. Vicinanza, D., Lauro, E.D., Contestabile, P., Gisonni, C., Lara, J.L., Losada, I.J.: Review of innovative harbor breakwaters for wave-energy conversion. J. Waterw. Port Coast. Ocean Eng. **145**, 03119001 (2019)
25. Marques Silva, J., Vieira, S.M., Valério, D., Henriques, J.C., Sclavounos, P.D.: Air pressure forecasting for the Mutriku oscillating-water-column wave power plant: review and case study. IET Renew. Power Generat. **15**(14), 3485–3503 (2021)
26. Hotta, H., Washio, Y., Yokozawa, H., Miyazaki, T.: R&D on wave power device "Mighty Whale." Renewable Energy **9**, 1223–1226 (1996)
27. Falcão, A.F., Cândido, J.J., Justino, P.A., Henriques, J.C.: Hydrodynamics of the IPS buoy wave energy converter including the effect of non-uniform acceleration tube cross section. Renewable Energy **41**, 105–114 (2012)
28. K. R. Tarrant, "Numerical modelling of parametric resonance of a heaving point absorber wave energy converter," Trinity College Dublin, 2015.
29. Wacher, A., Nielsen, K.: Mathematical and numerical modeling of the AquaBuOY wave energy converter. Mathemat.-Indus. Case stud. **2**, 16–33 (2010)
30. Ruellan, M., BenAhmed, H., Multon, B., Josset, C., Babarit, A., Clement, A.: Design methodology for a SEAREV wave energy converter. IEEE Trans. Energy Convers. **25**, 760–767 (2010)
31. P. Beirão, "Modelling and control of a wave energy converter: archimedes wave swing," Ph. D. thesis, Instituto Superior Técnico, 2007.
32. A. Henry, K. Doherty, L. Cameron, T. Whittaker, and R. Doherty, "Advances in the design of the Oyster wave energy converter," RINA Marine and Offshore Renewable Energy, London, UK, 2010.
33. Mehrangiz, S., Emami, Y., Sadigh, S.H.S., Etemadi, A.: Various technologies for producing energy from wave: a review. Int. J. Smart Grid Clean Energy **2**, 1–6 (2013)
34. Mehlum, E.: "Tapchan," in Hydrodynamics of Ocean Wave-Energy Utilization. Springer, USA (1986)
35. Vicinanza, D., Frigaard, P.: Wave pressure acting on a seawave slot-cone generator. Coast. Eng. **55**, 553–568 (2008)
36. Buccino, M., Dentale, F., Salerno, D., Contestabile, P., Calabrese, M.: The use of CFD in the analysis of wave loadings acting on seawave slot-cone generators. Sustainability **8**, 1255 (2016)
37. Tedd, J., Kofoed, J.P.: Measurements of overtopping flow time series on the wave dragon, wave energy converter. Renewable Energy **34**, 711–717 (2009)
38. L. Huang, Y. Li, D. Benites-Munoz, C. W. Windt, A. Feichtner, S. Tavakoli*, et al.*, "A review on the modelling of wave-structure interactions based on OpenFOAM," OpenFOAM® J. vol. 2, pp. 116–142, 2022.
39. Collins, I., Hossain, M., Dettmer, W., Masters, I.: Flexible membrane structures for wave energy harvesting: a review of the developments, materials and computational modelling approaches. Renew. Sustain. Energy Rev. **151**, 111478 (2021)
40. P. Rosa-Santos, F. Taveira-Pinto, M. López, and C. A. Rodríguez, "Hybrid Systems for Marine Energy Harvesting," vol. 10, ed: MDPI, 2022, p. 633.
41. Wang, K., Teng, H., Yang, P., Ng, H. D.: Numerical investigation of flow structures resulting from the interaction between an oblique detonation wave and an upper expansion corner. J. Fluid Mech. 903, **A28** (2020)
42. Wang, K., Zhang, Z., Yang, P., Teng, H.: Numerical study on reflection of an oblique detonation wave on an outward turning wall. Phys. Fluids **32**, 046101 (2020)
43. B. Zanuttigh, L. Margheritini, L. Gambles, and L. Martinelli, "Analysis of wave reflection from wave energy converters installed as breakwaters in harbour," In proceedings of the european wave and tidal energy conference (EWTEC), Uppsala, Sweden, 2009.
44. Thaha, A., Maricar, F., Aboe, A., Dwipuspita, A.: The breakwater, from wave breaker to wave catcher. Procedia Eng. **116**, 691–698 (2015)
45. Nabavi, S.F., Farshidianfar, A., Afsharfard, A., Khodaparast, H.H.: An ocean wave-based piezoelectric energy harvesting system using breaking wave force. Int. J. Mech. Sci. **151**, 498–507 (2019)
46. H. Chung and S. Chen, "Hydrodynamic mass," Argonne National Lab.1984.
47. C. Brennen, "A review of added mass and fluid inertial forces," BRENNEN (CE) SIERRA MADRE CA1982.
48. McCormick, M.E.: Ocean Engineering Mechanics: with Applications. Cambridge University Press, Cambridge (2009)
49. Biesheuvel, A.: Effectiveness of Floating Breakwaters-Wave Attenuating Floating Structures. Master of Science Thesis. Delft University of Technology, Netherlands (2013)
50. P. A. Leach, "Hinged floating breakwater : theory and experiments," Masters Thesis, Oregon State University.
51. Sell, N.P., Plummer, A., Hillis, A.J.: A Self-zeroing position controller for oscillating surge wave energy converters with strong asymmetry. J. Ocean Eng. Marine Energy **4**, 137–151 (2018)
52. Benites-Munoz, D., Huang, L., Anderlini, E., Marín-Lopez, J.R., Thomas, G.: Hydrodynamic modelling of an oscillating wave surge converter including power take-off. J. Marine Sci. Eng. **8**, 771 (2020)
53. Giannini, G., Temiz, I., Rosa-Santos, P., Shahroozi, Z., Ramos, V., Göteman, M., et al.: Wave energy converter power take-off system scaling and physical modelling. J. Marine Sci. Eng. **8**, 632 (2020)

54. Khalifehei, K., Azizyan, G., Gualtieri, C.: Analyzing the performance of wave-energy generator systems (SSG) for the southern coasts of Iran, in the Persian gulf and Oman sea. Energies **11**, 3209 (2018)